# *Single-Particle Time-of-Flight Mass Spectrometry Utilizing a Femtosecond Desorption and Ionization Laser*

# Single Particle Time of Flight Mass Spectrometry Utilizing a Femtosecond Desorption and Ionization Laser

Maria A. Zawadowicz[†], Ahmed Abdelmonem[‡], Claudia Mohr[‡], Harald Saathoff[‡], Karl D. Froyd[§ ||], Daniel M. Murphy[§], Thomas Leisner[‡], and Daniel J. Cziczo*[† ⊥]

[†]Department of Earth, Atmospheric and Planetary Sciences, Massachusetts Institute of Technology, 77 Massachusetts Ave., Cambridge, MA, 02139, USA.

[‡]Institute of Meteorology and Climate Research, Karlsruhe Institute of Technology, Karlsruhe, Germany

[§]NOAA Earth System Research Laboratory, Chemical Sciences Division, Boulder, CO 80305 USA

[||]Cooperative Institute for Research in Environmental Science, University of Colorado, Boulder, CO 80309 USA

[⊥]Department of Civil and Environmental Engineering, Massachusetts Institute of Technology, 77 Massachusetts Ave., Cambridge, MA, 02139 USA.

**ABSTRACT:** Single particle time of flight mass spectrometry has now been used since the 1990's to determine particle-to-particle variability and internal mixing state. Instruments commonly use 193 nm excimer or 266 nm frequency quadrupled Nd:YAG lasers to ablate and ionize particles in a single step. We describe the use of a femtosecond laser system (800 nm wavelength, 100 fs pulse duration) in combination with an existing single particle time-of-flight mass spectrometer. The goal of this project was to determine the suitability of a femtosecond laser for single particle studies via direct comparison to the excimer laser (193 nm wavelength, ~10 ns pulse duration) usually used with the instrument. Laser power, frequency and polarization were varied to determine the effect on mass spectra. Atmospherically relevant materials that are often used in laboratory studies, ammonium nitrate and sodium chloride, were used for the aerosol. The detection of trace amounts of a heavy metal, lead, in an ammonium nitrate matrix was also investigated. The femtosecond ionization had a large air background not present with the 193 nm excimer and produced more multiply charged ions. Overall, we find that femtosecond laser ablation and ionization of aerosol particles is not radically different than that provided by a 193 nm excimer.

Aerosol particles are important in the fields of atmospheric science, industrial manufacturing, human health and nanoparticle engineering. In atmospheric chemistry, they represent sites on which chemical reactions can take place, thus altering the chemical composition of the atmosphere.[1] In climate science they, and the clouds they spawn, are potential surfaces from which radiation can be scattered or on which it can be absorbed.[2] In industrial applications, particulates can represent unwanted sources of contamination that limit productivity, for example in pharmaceuticals and electronics.[3] In medicine, aerosol particles have been found to correlate with shorter life expectancy and ailments such as respiratory illnesses and cardiovascular disease.[4,5] In the field of nanoparticle engineering, submicron particles are fabricated for use in applications such as gas sensors or drug delivery.[6,7] In all of these areas, despite the diversity of topic, the efficacy of an aerosol particle – in chemistry, in radiative transfer, as a contaminant, and in terms of health effects – depends critically on its chemical composition.

During the 1990's, the field of aerosol science underwent a significant change when single particle mass spectrometers (SPMSs) were developed by several groups almost simultaneously. These instruments have been the subject of several previous review papers.[8–11] Among the salient advances, SPMSs allowed for analysis of small aerosol masses (~$10^{-15}$ g), differentiation of internally mixed component properties from refractory (e.g. mineral dust) to volatile (e.g. sulfuric and nitric acid, organic compounds) on a particle by particle basis both *in situ* and in real time.[12]

There are several almost universal components among the few dozen SPMSs that have been custom and commercially produced:[11] (1) an inlet system to draw the sample into the instrument and drop pressure for subsequent analysis, most often via differential pumping,

(2) a detection system, typically using photons scattered as particles pass through a continuous laser beam, (3) particle ablation and ionization, accomplished in "one step" (i.e., a single, pulsed, laser) or "two step" (i.e., separate ablation and ionization lasers) and (4) determination of chemical composition, typically via time-of-flight mass spectrometry.

The "one step" approach, where a single laser pulse both ablates the aerosol and ionizes the vaporized components,[9–11] is the most commonly used method in contemporary single particle mass spectrometry. For most field SPMS instruments, two laser wavelengths are typically used, 193 or 266 nm. UV wavelengths are preferred because they can ionize most atmospherically-relevant species[13,14] and the lasers of both wavelengths are commercially available with low volume (~.1 $m^3$), mass (~10 kg) and power (~100 W). Typically, those lasers are operated at ~10 ns pulse duration and 1-10 mJ pulse energy. With commonly used UV ionization lasers, the exact mechanisms of desorption and ionization of particles remain unresolved.[11,15,16] Higher pulse energies can be used (10-100 mJ), even with visible wavelengths, leading to ionization via plasma formation.

Peak power density was found to be important for the degree of fragmentation observed in the mass spectra. Silva and Prather[17] obtained organic spectra of pure PAH particles with very slight fragmentation, including the parent ion, using a 266 nm Nd:YAG laser at $10^8$ W/$cm^2$. The 193 nm excimer laser creates significant fragmentation and some atomic high-energy ions (e.g. $Na^-$, $Na_2^+$) at a peak power density of ~$10^9$ W/$cm^2$. With reduced excimer power, there is less fragmentation and some parent ions for organic species. Reents and Schabel[18] obtained spectra with only atomic ions and no fragments or clusters at a peak power density of $10^{10}$ W/$cm^2$ using a 532 nm Nd:YAG laser. Similarly, Wang and Johnston[19] use a 532 nm Nd:YAG laser with 169 mJ pulse energy and $10^{10}$ W/$cm^2$ peak power density to ionize small particles by plasma production, resulting in spectra consisting of only atomic ions, both singly and multiply charged.

Peak power density can be varied by changing the pulse energy, as in the examples provided above, or by changing the pulse duration. The effect of pulse duration on SPMS mass spectra has not been studied previously. Here we describe the use of a femtosecond laser (800 nm fundamental wavelength, 100 fs pulse duration) coupled to an existing SPMS, the Particle Analysis by Laser Mass Spectrometry (PALMS) instrument.[12]

In addition to providing insight into the effect of pulse duration on single particle ionization, using femtosecond pulses can provide additional analytical advantages for SPMS. When femtosecond laser pulses interact with matter, nonlinear optical effects can arise. These effects have been used in many fields including, but not limited to, atomic scale resolution in tunneling microscopy,[20] high harmonic generation,[21] chemical dynamics studies using fast spectroscopic techniques[22] and surface probing using second harmonic generation.[23,24]

Femtosecond lasers have been successfully used in laser ablation mass spectrometry of solid samples.[25,26] It has been shown that using low-fluence femtosecond pulses to ablate solid samples in vacuum allows evaporation from very localized sites, as little as a few nanometers across, thereby enabling high-resolution depth profiling of layered samples.[25] Femtosecond ablation and ionization of dried organic solutions on substrates has been found to lead to a complete fragmentation of the sample, producing only atomic ions, in contrast to nanosecond ablation and ionization, which produces fragment ions and clusters.[27,28] This complete ionization occurs because of plasma formation as a result of the intense laser pulse.[27]

In organic vapors, in contrast to solid targets, femtosecond ionization can reduce fragmentation, thus making the identification of mass spectral peaks simpler.[29,30] In contrast to nano- and pico-second pulses, a femtosecond pulse is able to bypass dissociation channels during the excitation processes.[29] Saturation ionization, a condition when all molecules present in the laser focus have been ionized, can occur for organic molecules irradiated with femtosecond laser pulses, which makes the technique highly sensitive and quantitative.[30,31] Laser intensity, wavelength and polarization have all been found to influence the fragmentation of organic molecules.[29,32] Studies of ionization of vapors and gases are likely not directly applicable to ionization of bulk samples or small particles *in vacuo* because of different physics involved in the processes.

The experiment described here aims to demonstrate feasibility of combining a femtosecond laser with existing SPMS technology and investigate the amount of fragmentation resulting from ionization with shorter pulses. Answering these questions will provide insight into feasibility of using a femtosecond laser as a depth profiling tool for atmospheric aerosol.

We describe experiments on the effect of laser power, wavelength, pulse length and polarization variation on mass spectra. Atmospherically relevant materials, ammonium nitrate ($NH_4NO_3$) and sodium chloride (NaCl), the former with and without a trace metal, lead, were used for the aerosol and compared to spectra obtained using the traditional PALMS with an excimer laser (193 nm wavelength, ~10 ns pulse duration).

## 2. Experimental Methods

The PALMS instrument focuses incoming particles using an aerodynamic inlet[33–35] and a set of differential pumping stages. A full description of PALMS is provided in Cziczo et al.[12] In brief, particle detection and aerodynamic sizing occurs as particles pass through two 532 nm frequency doubled Nd:YAG laser beams (PALMS sizing laser in Figure 1) and scatter light. The beams are set a known distance apart, 34 mm, which allows for accurate aerodynamic sizing, as the aerodynamic lens

accelerates particles to a size-dependent velocity. This velocity is measured as the transit time between the laser beams and compared to calibrated values for polystyrene latex (PSL) spheres of unit density and a specific size. The 193 nm excimer laser is triggered by a scattering event detected on the second Nd:YAG laser beam and timed to strike the particle in the "one step" method that ablates and ionizes the components. The laser, a PSX-100 excimer laser (MPB Technologies) nominally delivers 5 mJ per pulse with a ~3 ns width and can operate up to 100 Hz. In practice, spectral data recording limits acquisition to ~8 Hz and the measured pulse energy delivered to the source region is 2 mJ. Depending on the polarity of extraction plates, either positive or negative ions are accelerated into a reflectron time of flight mass spectrometer where they are detected with a microchannel plate (MCP). Particle vacuum aerodynamic diameter and chemical composition are measured *in situ* and in real time at the single particle level. Due to highly variable ionization efficiencies and matrix effects of common atmospheric materials and mixtures, SPMSs such as PALMS are not normally considered quantitative without calibration[36] although trends in ion signal have been used as an indication of relative abundance.[11,37]

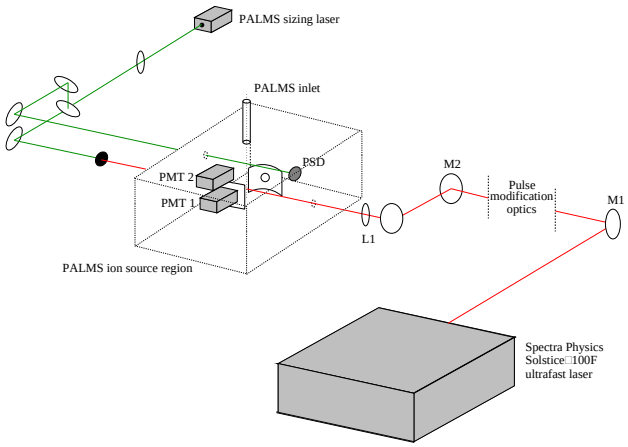


Figure 1. Schematic diagram of the femto-PALMS experiment. Note that the traditional PALMS excimer laser would occupy the volume to the upper right in the figure. For these experiments it has been replaced with a femtosecond laser (Spectra Physics Solstice-100F) with the beam directed into the PALMS ion source region using two mirrors (M1 and M2) and a lens (L1).

For this study, PALMS was modified by decoupling the excimer laser and replacing it with a Ti:Sapphire femtosecond laser system (Spectra Physics Solstice–100F Ultrafast Laser), hereafter termed "the femtosecond laser". The femtosecond laser has a fundamental wavelength of 800 nm, 3.5 mJ pulse energy, ~100 fs pulse width and 1 kHz repetition rate. The beam profile is close to Gaussian with beam quality factor, $M^2 < 1.3$ ($M^2 = 1$ for an ideal Gaussian beam).

Hereafter, we term the combined femtosecond laser and PALMS as "femto-PALMS". Several changes were made to the existing hardware in order to use the femtosecond laser as the PALMS ionization and ablation laser. During normal operation, the PALMS excimer laser is triggered to fire by pulses detected at a photomultiplier tube (PMT), which are produced by particles focused into the instrument by the aerodynamic inlet which scatter light from a 532 nm sizing laser beam (PMT 1 in Figure 1). The excimer trigger also begins the acquisition of the mass spectrum as ions are created in the PALMS ion source region. In the femto-PALMS experiment, an external triggering pulse from the femtosecond laser, coinciding with its firing, was provided to the PALMS trigger hardware to begin spectrum acquisition. This results in a significantly different mode of operation from that traditionally used for PALMS mass spectrum acquisition. Instead of a particle light scattering event starting the data acquisition process, femto-PALMS was run in a "free fire" mode where the fortuitous presence of a particle in the ionization and ablation region at the time the femtosecond laser fired resulted in mass spectral acquisition. While the trigger pulse frequency was 1 kHz in sync with the laser, the maximum PALMS data acquisition rate is limited at ~8 Hz by writing mass spectral data to the instrument computer, and this set the data acquisition rate. Concentrations in front of the PALMS inlet used in this experiment ranged from 1 to 3 × $10^4$ particles/$cm^3$ and, with optimized optical alignment, 0.2% to 1% of acquired spectra have a signal consistent with a particle in the beam (see next sections for additional information). The hit rate is comparable to that of traditional PALMS run with the excimer laser under similar particle loading conditions.

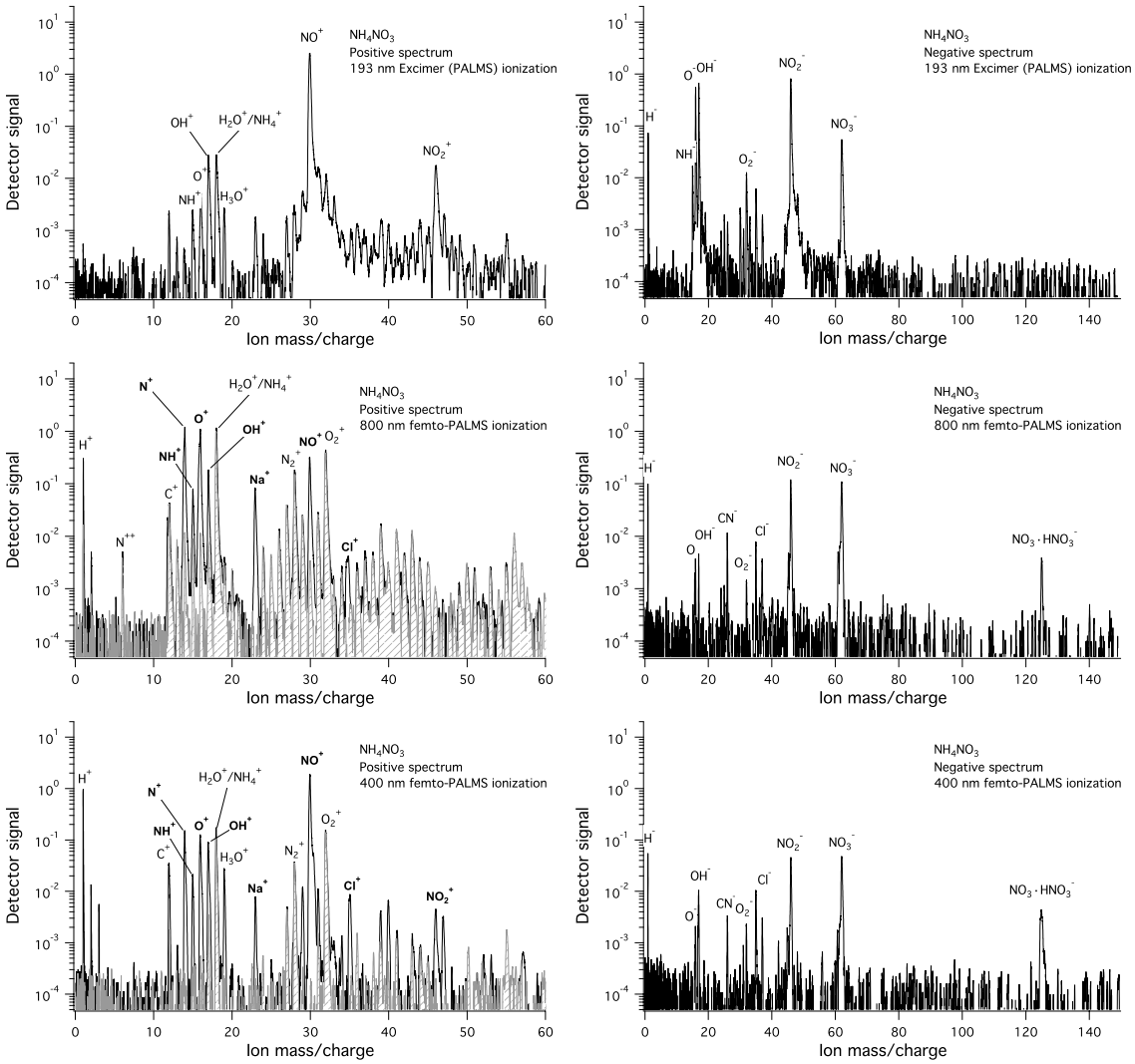


Figure 2. Representative positive and negative spectra of $NH_4NO_3$ acquired with PALMS using a 193 nm excimer laser (top panel), with femto-PALMS using a 800 nm femtosecond laser (middle panel) and with femto-PALMS using a frequency doubled femtosecond laser at 400 nm (bottom panel). Hatched areas for positive femto-PALMS spectra represent background peaks not associated with $NH_4NO_3$ particles. Peaks associated only with $NH_4NO_3$ particles are labeled in bold type.

A custom optical pathway was constructed between the femtosecond laser and PALMS. Two mirrors (M1 and M2) were mounted on the optical table, which supported the laser to redirect the beam. Two clamps were bolted between the femtosecond laser table and PALMS so that the optical path remained fixed. Lens L1, with 20 cm focal length, was used to focus the femtosecond laser beam into the PALMS ion source region at the same diameter (~250 μm) at the location of the particle beam from the aerodynamic lens as the traditional PALMS excimer laser. With the nominal pulse energy of 3.5 mJ and pulse duration of 100 fs, the peak power density of the femtosecond laser at the focus is $7 \times 10^{13}$ W/cm$^2$. This is five orders of magnitude more than the peak power density produced by the excimer laser at the same focus (~$9 \times 10^8$ W/cm$^2$) although the energy densities were similar (~6 J/cm$^2$). The lens was mounted on an x-y-z micrometer stage to enable positioning of the focus. This position was realigned for each experiment by optimizing particle ionization frequency. The experiments described here were carried out over the course of eight days at the Karlsruhe Institute of Technology in Karlsruhe, Germany with experiments conducted after daily realignment of the laser to maximize hit rate.

The optical path also allowed for experiments that varied the femtosecond laser wavelength, pulse stretching, polarization and power: (1) 800 and 400 nm experiments were conducted by placing a second harmonic generator (SHG) between M1 and M2, (2) three plates of glass were inserted between M1 and M2 for experiments involving spatial pulse stretching, (3) a three-mirror polarization rotator was inserted between M1 and M2 to change the femtosecond laser beam polarization by 90° and (4) M2 was replaced by beam splitters to produce pulses at 70%, 50%, and 30% of full power.

Test particles for femto-PALMS were produced by nebulizing solutions of NaCl (≥ 99.5%, Merck), $NH_4NO_3$ (≥ 99.5%, Fluka), or $Pb(NO_3)_2$ (≥ 99.5%, Merck) mixed at

known concentration with $NH_4NO_3$. Ultrapure water (18 MΩ·cm, Barnstead Nanopure Infinity, Werner Reinstwassersysteme) was used as the solvent. Particles were produced with a custom Collison atomizer and dried by passing the flow through a diffusion drier filled with silica gel (Merck). All femto-PALMS experiments were performed with 240 nm electrical mobility diameter particles (peak in number size distribution produced by atomizer) selected by a differential mobility analyzer (DMA 3081, TSI). The particles were size-selected to limit number concentrations produced by the atomizer. The number concentrations were kept at ~$10^4$ particles/$cm^3$ in order to avoid clogging the PALMS skimmers and minimize clogging of the PALMS critical orifice. Traditional PALMS spectra shown for comparison were polydisperse, produced by nebulizing solutions of NaCl (≥99.0%, Macron) or $NH_4NO_3$ (≥99.0%, Sigma-Aldrich) in Milli-Q water (18.2 MΩcm, Millipore, Bedford, MA). Due to the sensitivity of traditional PALMS, a medical nebulizer (Briggs Healthcare, Waukegan, IL), which produced a lower concentration of particles, was used.

## 3. Results and Discussion

### 3.1 Instrument Background

Positive and negative polarity spectra were acquired for $NH_4NO_3$ and NaCl particles with both traditional PALMS and femto-PALMS. Results are detailed in the following sections. For both particle types, positive femto-PALMS spectra, such as those shown in Figure 2 for $NH_4NO_3$, exhibit a background larger than that observed for PALMS (note that the background is marked with a hatch pattern in Figure 2). In cases where the ionization region does not contain an aerosol particle, both the excimer and femtosecond lasers still created ions, which constitute this background.

The abundance of air background ions was maximized by moving the laser focus inside the ionization region, which is also consistent with air beam ionization. An example of a femto-PALMS air beam background (i.e., a spectrum devoid of features attributable to a particle) is shown in Figure 3. It contains both singly and multiply charged ions. The presence of singly ($N^+$, $O^+$) and multiply charged ($O^{++}$, $N^{++}$) ions in the background could suggest plasma formation at the focus. Note that a laser focus alignment that maximized the production of background ions did not coincide with high particle hit rates. In traditional PALMS excimer ionization a background is also present, but it is primarily organic in nature. In both cases, the mass scales of background spectra match the mass scales of particle spectra, suggesting that the background ions are created at the usual ion extraction point and do not result from surface reflections inside the ionization region. In traditional PALMS, the organic background accounts for 0.3 - 1% of the total positive ion current, measured as mA at the MCP.

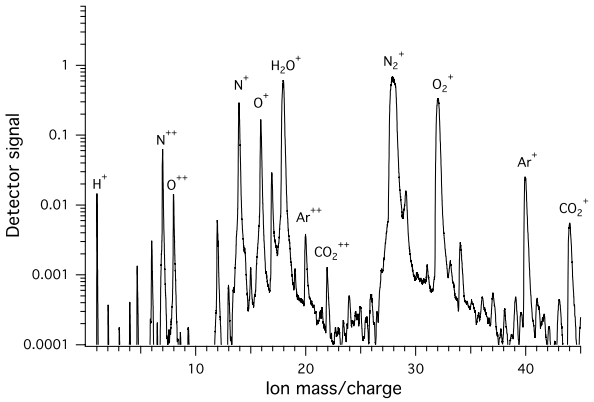


FIGURE 3. Spectrum of the air background created by the femtosecond laser. Note the presence of atomic singly and doubly charged ions.

For femto-PALMS the air background accounts for 30 - 60% of the positive ion current, on average. Background ions were not observed with either laser in negative polarity.

The background signal was found to be a secondary indication of the quality of laser alignment and the experiments reported here are only those with minimized background and maximized particle hit rate. With this restriction, 221 particle spectra for NaCl, 413 for $NH_4NO_3$ and 190 for $NH_4NO_3$ doped with Pb form the basis of this discussion.

### 3.2 $NH_4NO_3$ Aerosol Particles

$NH_4NO_3$ mass spectra obtained with femto-PALMS at two wavelengths — the 800 nm fundamental and 400 nm second harmonic — are shown in Figure 2. Mass assignment in femto-PALMS spectra required refitting the mass scale because the position of the femtosecond laser focus was not exactly matched to the position of the excimer beam focus. An initial observation is that the spectra generated are similar, despite the different laser pulse durations, powers and wavelengths. The most obvious differences are a lack of a strong $NO_2^+$ peak in femto-PALMS spectra, which is present in PALMS, and the presence of $N^+$ and $NO_3HNO_3^-$ in the femto-PALMS spectra, but not PALMS. As a whole, these are minimal differences and imply similar ionization processes despite the different lasers.

As noted in the previous section, the interpretation of positive femto-PALMS spectra is complicated by the presence of the air background. A typical background spectrum for both laser wavelengths is plotted over the positive femto-PALMS spectra and highlighted with a hatch pattern. The ions that are not found in the background or enhanced by the presence of $NH_4NO_3$ particles, are +14, +15, +16, +17, +23, +35 and +30, corresponding to $N^+$, $NH^+$, $O^+$, $OH^+$, $Na^+$, $Cl^+$ and $NO^+$ (labeled in bold type in Figure 2). Sodium and chlorine ions are present due to trace amounts, which remained in

the aerosol generation system between experiments.

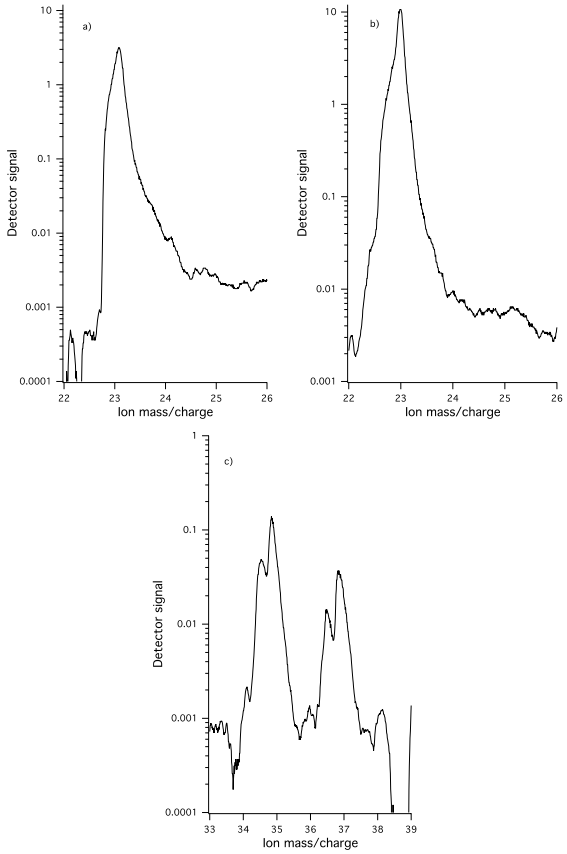


FIGURE 4. Peak shapes characteristic of PALMS and femto-PALMS. Panel a) $Na^+$ peak characteristic of traditional PALMS. Panel b) $Na^+$ peak characteristic of femto-PALMS. Panel c) $^{35}Cl^+$ and $^{37}Cl^+$ peaks characteristic of femto-PALMS. Note the split peak shape discussed in the main text.

Femto-PALMS spectra of $NH_4NO_3$ tend to be lower in total signal than those taken with the excimer laser. Total ion currents for positive and negative spectra were measured and are discussed in the following section.

Peak shapes in femto-PALMS and PALMS are alike and this, with the similarity in ions generated, further suggests comparable ionization processes. Typical peak shapes of PALMS and femto-PALMS are shown in Figure 4. Note the similarity in $Na^+$ peak shapes in the top panel. One exception is that some of the peaks in femto-PALMS spectra have a low mass "shoulder" (e.g., $NO_2^-$ and $NO_3^-$ in Figure 2 and $^{35}Cl^+$ and $^{37}Cl^+$ in the bottom panel of Figure 4), an effect infrequent for PALMS. The shoulders could be due to either a very energetic ion formation mechanism, space charge effects in the ion source, or unimolecular decomposition of ions within the ion source or possibly the reflectron. We do not believe there is enough information to determine the exact mechanism at this time.

3.2.1 Laser Power Variation

Spectra of $NH_4NO_3$ were taken at four average laser powers and the generated ion current for each experiment is summarized in Figure 5. The average power of the femtosecond laser was reduced to 70%, 50% and 30% of full by attenuating the beam with three beam splitters. The average laser power at each attenuation was measured after propagation through the focusing lens (L1 in Figure 1) with a power meter. Values between 2.99 W (for no attenuation) and 0.53 W (for 70% attenuation) were measured. Pulse energies, shown on the x-axis of Figure 5, were obtained by dividing the measured average laser power by the laser repetition rate of 1 kHz. Using a pulse duration of 100 fs, those pulse energies corresponded roughly to peak power densities between 1 and $6 \times 10^{13}$ W/cm² at the laser focus in the source region. The ion currents recorded at the MCP for the different pulse energies are given for positive and negative spectra on the left and right y-axes in Figure 5, respectively. At reduced pulse energies ions remained the same as those given in Figure 2 but with reduced signal.

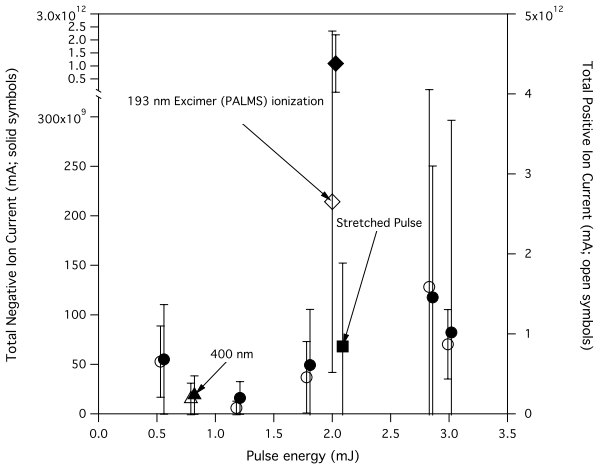


FIGURE 5. Average total ion current (mA) generated per spectrum of $NH_4NO_3$ as a function of laser power. Solid circles represent negative polarity data (left axis) while open circles represent positive polarity data (right axis). Ion current data for a negative polarity experiment where the pulse length was stretched from 100 to 104 fs are shown with a solid square. Ion current data for experiments where frequency doubling to 400 nm was utilized are shown with triangles. Ion current data for traditional PALMS with a 193 nm excimer laser are shown for comparison with diamonds. Negative polarity data are offset in power (+ 0.03 W) to avoid overlap of error bars

Negative ion current was, on average, an order of magnitude lower than positive ion current. Partially, this is accounted for by the background generated in positive spectra. For most points shown in Figure 5 (with the exception of those at 2.83 mJ), the background ion current was 60% of the total positive ion current. This is significant but does not fully explain the difference of an order of magnitude between positive and negative, implying a higher average signal, regardless of background, in positive mode. For comparison, Figure 5 provides ion current for $NH_4NO_3$ from traditional PALMS. The total positive ion current in PALMS is 2.4 times larger than negative, which is accounted for by the electrons

extracted during the ionization process that are not measured by PALMS.

Excimer laser ionization has a power density threshold for ion production, which varies for particle composition and laser wavelength.[13] Thresholds for ion production have previously been studied for the PALMS 193 nm excimer laser by Thomson et al.[13,14] At power densities higher than the threshold, the ion yield is not typically linear with increasing power density.[14] Thomson, et al.[14] measured the ion production threshold for $NH_4NO_3$ ionized with the 193 nm excimer laser to be $5.6 \times 10^6$ W/cm² for positive ions and $5.3 \times 10^6$ W/cm² for negative ions. In the femto-PALMS dataset presented in Figure 5, no clear threshold is present. This indicates that the threshold, if present, is lower than $1 \times 10^{13}$ W/cm² since both positive and negative ions are still produced at 0.5 mJ. Because the ion production as a function of power density is expected to be nonlinear, the threshold cannot be deduced by a simple linear fit through the data.

In Figure 5, error bars in femto-PALMS and PALMS data represent the range of ion currents generated by different particles and are of the same order. Differences in the PALMS data can be attributed to excimer shot-to-shot energy variability and to the non-constant position of particles within the profile of the laser beam. The latter is a particular challenge for the excimer laser because the beam is not Gaussian and local "hot spots" are possible.[11] The femtosecond laser beam is closer to Gaussian and there should be less spatial variability. Improvement in the beam quality of the femtosecond laser is apparently offset by alignment fluctuations and/or the particle position within the Gaussian profile of the beam. As an example, the data taken at 2.83 and 2.99 mJ were taken on different days and highlight this variability. For the point at 2.83 mJ, the background accounted for 30% of the total ion current in positive polarity whereas it represented 60% during the 2.99 mJ experiments. We suggest future experiments need to consider the reproducibility of the femtosecond laser alignment to minimize day-to-day variability.

The femtosecond pulses were dispersively broadened by 4% in one experiment. The ion current is reported in Figure 5 and no differences in the kinds of ions produced were found.

3.2.2 Laser Wavelength Variation

Wavelength has been found to be an important consideration for the ion production threshold when considering traditional SPMSs. For atmospherically-relevant species, 193 nm excimer ionization thresholds are lower than those for longer wavelengths, such as a 266 nm Nd:YAG laser.[11,14]

Spectra of $NH_4NO_3$ were obtained with the femtosecond laser frequency-doubled to 400 nm (Figure 5). Examples of spectra generated are also shown in Figure 2. Changes in the spectra with wavelength were small. The air background at 400 nm is lower in intensity although this may correlate with the lower power inherent in second harmonic generation (the average power of the 400nm beam used for these experiments was 0.79 W). Differences in the relative intensities of peaks such as $NO^+$ compared to $NO_2^+$ were smaller on average between 400 and 800 nm than the shot-to-shot variability at either wavelength.

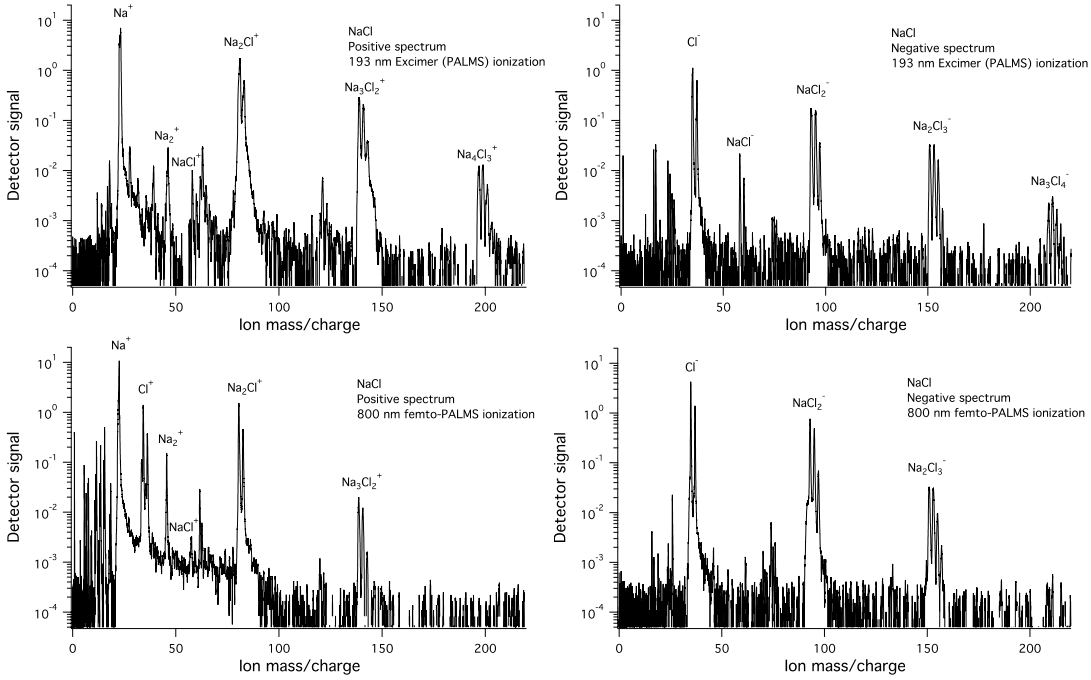


FIGURE 6. Representative positive and negative spectra of NaCl acquired with PALMS (top panel) and with femto-PALMS (bottom panel).

3.3. NaCl Aerosol Particles

Femto-PALMS and PALMS spectra of NaCl aerosol particles are compared in Figure 6. The femto-PALMS spectra in Figure 6 were taken at 2.86 W average power and 800 nm wavelength. The significant difference between PALMS and femto-PALMS spectra is the presence of $Cl^+$ ions at +35 and +37. Those ions do not appear in any positive PALMS NaCl spectrum taken for this work or previously. $Cl^+$ ions require high energies to produce since the first ionization potential of chlorine is 13 eV (whereas the first ionization potential of sodium is 5.1 eV). In femto-PALMS, $Cl^+$ ions are present in ~50% of the spectra. When present, the $Cl^+$ peaks are large (on the order of 10-20% of the total positive ion current). Additionally, the $Cl^+$ features are associated with the presence of wide and/or split peaks (Figure 4), similarly to $NO_2^-$ and $NO_3^-$ for $NH_4NO_3$ in Figure 2. These observations may be indicative of a different ionization mechanism for chlorine, or possibly two distinct mechanisms. The power density is highest at the focus of the femtosecond laser beam although particles hit when outside the focus should still experience suitable power density to ionize most species. Less common ions may be associated with particles ablated and ionized at or nearer the beam focus (i.e., peak power). Another noteworthy difference is that femto-PALMS spectra do not exhibit high mass ions at the same frequency as PALMS spectra. For example, the $Na_4Cl_3^+$ and $Na_3Cl_4^-$ ions are generated in 40% of the PALMS spectra, but only 1% of femto-PALMS spectra. This is also consistent with harder ionization in femto-PALMS.

As in the case of $NH_4NO_3$, femto-PALMS fragmentation patterns for NaCl are similar to fragmentation patterns of traditional PALMS with an excimer laser. Femto-PALMS spectra are, however, unlike spectra acquired with higher energy nanosecond pulses reported previously in literature. For example, Reents and Ge[38] obtained positive NaCl spectra with a Nd:YAG laser operated simultaneously at 532 and 1064 nm and 300 mJ pulse energy. The Reents and Ge spectra consisted only of atomic ions ($Na^+$, $Cl^+$) and their doubly charged equivalents. Reents and Schabel,[18] using a 532 nm Nd:YAG at 93 mJ pulse energy, obtained similar spectra to Reents and Ge.[38] Peak power densities in those experiments were $1 \times 10^{10}$ W/cm$^2$, between that of PALMS and femto-PALMS. The pulse energy used by Reents and Ge[38] was larger, by two orders of magnitude, than that of PALMS or femto-PALMS. At this time, the degree of fragmentation appears related to the pulse energy, not the peak power density. The reason is unclear, although it may be indicative of the criticality of alignment of the laser focus with the particle beam (i.e., the actual power density experienced by the particle).

Average total ion currents for NaCl were the same (within uncertainty) for both positive and negative spectra for PALMS and femto-PALMS. For femto-PALMS, the total positive and negative ion currents at 2.86 mJ pulse energy were 4.4 (± 3.4) × $10^{12}$ and 1.2 (± 1.1) × $10^{12}$ mA, respectively. For PALMS, total positive and negative ion currents were 5.8 (± 2.0) × $10^{12}$ and 8.6 (± 6.7) × $10^{11}$ mA, respectively. Fewer than 10 spectra were acquired at 30% power at each polarity with femto-PALMS. Allowing for the variability in alignment and particle-to-particle differences, the exact trend in ion current signal versus power remains uncertain.

The polarization of the femtosecond laser was rotated by 90°, without a change in average power, for some NaCl experiments. No effect on the spectral appearance or the total ion current was observed. These experiments were conducted because a change in pulse polarization will change the direction of the initial kinetic energy of the ions. This does not appear to have an effect on the mass spectra.

### 3.3 Sensitivity of femto-PALMS to lead in $NH_4NO_3$ particles

PALMS is sensitive to trace metallic species, with one atmospherically-relevant example being lead. Murphy et al.[39] showed that a lead concentration calibration (i.e., a PALMS sensitivity to lead) could be obtained from laboratory data in order to infer concentrations in field data. The laboratory calibration data determined by Murphy et al.[39] are shown in Figure 7 (open diamonds). The calibration data were repeated for this work using femto-PALMS where lead was added in known quantities to an $NH_4NO_3$ matrix. Solutions of lead at a range of concentrations (0.09% - 1.20% by weight) were prepared in aqueous solutions of $NH_4NO_3$, and then atomized, dried and analyzed with femto-PALMS. The elemental lead peaks in the mass spectra were integrated and the resulting areas were compared to the total ion current after background subtraction, the same methodology used by Murphy et al.[39]

Both PALMS and femto-PALMS are more sensitive to lead than to $NH_4NO_3$, which can be inferred from the positive slopes in Figure 7. PALMS exhibits 27 times higher sensitivity than femto-PALMS. We note that the femto-PALMS signal appears to vary significantly with laser alignment and that the point with the highest lead content (1.2%) was taken during a period of high relatively background (50%, compared to ~35% for other points). Overall, the data suggest that the limit of detection of lead in femto-PALMS is between 0.09% and 0.17% dry particle lead content.

## 4. Conclusions and Future Work

A femtosecond laser was coupled to an existing SPMS and compared to traditional excimer laser 1-step ablation and ionization. The lasers considered in this work, a 193 nm excimer laser and a 800nm/400nm femtosecond laser, have similar pulse energies, 2-4 mJ. They differ significantly, however, in wavelength, pulse duration and peak power. The femtosecond laser experiments had five order of magnitude greater power density and yet produced similar fragmentation patterns. Mass spectra of $NH_4NO_3$ and NaCl were similar for PALMS and femto-

PALMS with the exception of $N^+$, $O_2^+$ and $Cl^+$ ions, which are not normally produced with a 193 nm excimer, and the $NO_2^+$ ion which is present only in PALMS spectra. The production of the high energy atomic ions suggests that there are some differences in ionization mechanisms, especially noteworthy in the case of $Cl^+$ production. Having considered only two relatively simple particle types here, we note that future work may find more significant differences if more complex particles (e.g. mixed organics and inorganics) are considered.

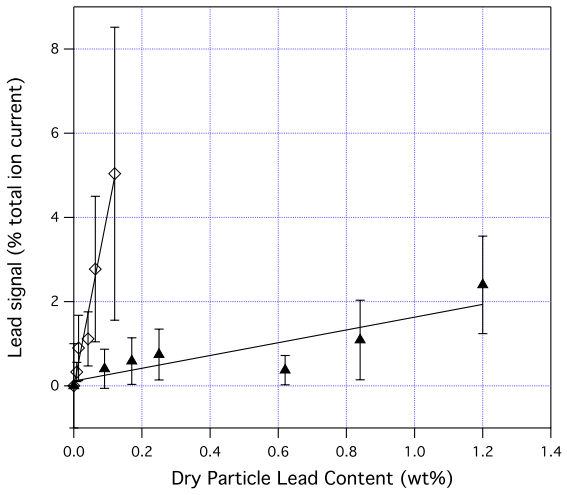


FIGURE 7. Sensitivity of the signal of the lead isotope at mass 208 (in percentage of total ion current generated) to the dry particle mass content (in weight percent) where $NH_4NO_3$ was used as the matrix. Solid triangles represent data acquired with femto-PALMS and traditional PALMS data are open diamonds. PALMS data are reproduced from Murphy et al.[34] Error bars indicate the range of signals in the single particle data.

The high energy ions ($Cl^+$, $N^+$) evident in femto-PALMS are similar to spectra obtained with higher pulse energy (~100 mJ) ionization lasers that produce ions through plasma formation, such as that used by Wang and Johnston.[19] At this time it is unclear why the pulse energy, and not the peak power density, appears to correlate with the fragmentation. Simulations by Zhou et al.[40] show that in plasma-formation regime, ablation and ionization is complete before the ionizing pulse reaches its peak intensity, which suggests that pulse length plays a limited role in the ionization process. However, ion clusters (e.g. $NO^+$, $Na_2Cl^+$) present in femto-PALMS spectra point to a more complex ionization mechanism than only plasma formation and the Zhou et al.[40] results should be applied with caution. In order to experimentally investigate this correlation, pulse energy should be varied over a large range (1-100 mJ) under the same pulse duration and wavelength conditions.

Femto-PALMS was found to produce background ions consistent with ionization of the air beam. The air background consisted of atomic ions, both singly and multiply charged, which is similar to the background described by Wang and Johnston[19] for a plasma ionization technique. Wang and Johnston[19] found that the background signal was higher when a particle was present in the beam than in the absence of a particle, suggesting that plasma electrons play a role in background ionization. No such effect was found here. Characterizing this air beam background with a closed and/or filtered inlet (i.e., when no particles are present) is suggested as an area of future interest.

Ionization laser wavelength has been shown to be an important consideration related to the ionization onset when considering UV lasers.[13] Power densities used in this experiment were, in all cases, above the ionization threshold for NaCl and $NH_4NO_3$ despite the longer femtosecond laser wavelength. Dispersive broadening of the pulses and polarization of the femtosecond laser did not produce a significant change in the mass spectra or ion current. We suggest the effect of pulse broadening and circular and elliptical polarization as areas for future study. Additionally, using lower laser power densities or aerosols that are harder to ionize (e.g. sulfates) would enable determination of ionization threshold and comparison across ionization wavelengths.

Quantification of the femto-PALMS sensitivity to lead in a $NH_4NO_3$ matrix showed a lower sensitivity when compared to PALMS. Sensitivity to other heavy metals in other matrixes represents an area of interest in future experiments.

Femtosecond laser ablation has been successfully used for depth profiling of layered samples because it ablates small quantities of material from localized spots.[25,26] Surface sensitivity and the potential for depth profiling of aerosol particles was not studied in this experiment. If this could be translated to depth-profiling of single aerosol particles it would represent a useful tool. For example, it could represent a means to study the morphology of phase-separated aerosols which are known to occur in many mixed organic-inorganic aerosols.[41] In order to investigate this, a method to reproducibly align the femtosecond laser focus relative to the particle beam must first be developed.

## AUTHOR INFORMATION

### Corresponding Author

*Email: djcziczo@mit.edu

### Notes

The authors declare no competing financial interest.

## ACKNOWLEDGMENT

This research was supported by NSF Grant 023693-001, MIT and KIT internal funding. D. J. C. acknowledges the support of the Victor P. Starr Career Development Chair at MIT. M. A. Z. acknowledges the support of a NASA Earth and Space Science Fellowship.

## REFERENCES

(1) George, I. J.; Abbatt, J. P. D. *Nat Chem* **2010**, *2* (9), 713–722.
(2) Ramanathan, V.; Crutzen, P. J.; Kiehl, J. T.; Rosenfeld, D. *Science* **2001**, *294* (5549), 2119–2124.
(3) Cooper, D. W. *Aerosol Sci. Technol.* **1986**, *5* (3), 287–299.
(4) Dockery, D. W.; Pope, C. A.; Xu, X.; Spengler, J. D.; Ware, J. H.; Fay, M. E.; Ferris, B. G.; Speizer, F. E. *N. Engl. J. Med.* **1993**, *329* (24), 1753–1759.
(5) Miller, K. A.; Siscovick, D. S.; Sheppard, L.; Shepherd, K.; Sullivan, J. H.; Anderson, G. L.; Kaufman, J. D. *N. Engl. J. Med.* **2007**, *356* (5), 447–458.
(6) Panchapakesan, B.; DeVoe, D. L.; Widmaier, M. R.; Cavicchi, R.; Semancik, S. *Nanotechnology* **2001**, *12* (3), 336–349.
(7) Hu, J.; Johnston, K. P.; Williams, R. O. *Drug Dev. Ind. Pharm.* **2004**, *30* (3), 233–245.
(8) Johnston, M. V. *J. Mass Spectrom.* **2000**, *35* (5), 585–595.
(9) Noble, C. A.; Prather, K. A. *Mass Spectrom. Rev.* **2000**, *19* (4), 248–274.
(10) Coe, H.; Allan, J. D. In *Analytical Techniques for Atmospheric Measurement*; Heard, D. E., Ed.; Blackwell Publishing, 2006; pp 265–311.
(11) Murphy, D. M. *Mass Spectrom. Rev.* **2007**, *26* (2), 150–165.
(12) Cziczo, D. J.; Thomson, D. S.; Thompson, T. L.; DeMott, P. J.; Murphy, D. M. *Int. J. Mass Spectrom.* **2006**, *258* (1--3), 21–29.
(13) Thomson, D. S.; Murphy, D. M. *Appl. Opt.* **1993**, *32* (33), 6818–6826.
(14) Thomson, D. S.; Middlebrook, A. M.; Murphy, D. M. *Aerosol Sci. Technol.* **1997**, *26*, 544–559.
(15) Carson, P. G.; Johnston, M. V.; Wexler, A. S. *Rapid Commun. Mass Spectrom.* **1997**, *11* (9), 993–996.
(16) Reinard, M. S.; Johnston, M. V. *J. Am. Soc. Mass Spectrom.* **2008**, *19* (3), 389–399.
(17) Silva, P. J.; Prather, K. A. *Anal. Chem.* **2000**, *72* (15), 3553–3562.
(18) Reents, W. D.; Schabel, M. J. *Anal. Chem.* **2001**, *73* (22), 5403–5414.
(19) Wang, S.; Johnston, M. V. *Int. J. Mass Spectrom.* **2006**, *258* (1-3), 50–57.
(20) Tersoff, J.; Hamann, D. R. *Phys. Rev. B* **1985**, *31* (2), 805–813.
(21) Schafer, K. J.; Kulander, K. C. *Phys. Rev. Lett.* **1997**, *78* (4), 638–641.
(22) Shim, S.; Mathies, R. A. *J. Raman Spectrosc.* **2008**, *39* (11), 1526–1530.
(23) Petersen, P. B.; Saykally, R. J. *J. Phys. Chem. B* **2006**, *110* (29), 14060–14073.
(24) Abdelmonem, A.; Lützenkirchen, J.; Leisner, T. *Atmos. Meas. Tech.* **2015**, *8* (8), 3519–3526.
(25) Margetic, V.; Niemax, K.; Hergenröder, R. *Anal. Chem.* **2003**, *75* (14), 3435–3439.
(26) Hergenröder, R.; Samek, O.; Hommes, V. *Mass Spectrom. Rev.* **2006**, *25* (4), 551–572.
(27) Kurata-Nishimura, M.; Tokanai, F.; Matsuo, Y.; Kobayashi, T.; Kawai, J.; Kumagai, H.; Midorikawa, K.; Tanihata, I.; Hayashizaki, Y. *Appl. Surf. Sci.* **2002**, *197-198*, 715–719.
(28) Kato, T.; Kobayashi, T.; Matsuo, Y.; Kurata-Nishimura, M.; Oyama, R.; Matsumura, Y.; Yamamoto, H.; Kawai, J.; Hayashizaki, Y. *J. Phys. Conf. Ser.* **2007**, *59*, 372–375.
(29) Nakashima, N.; Yatsuhashi, T. In *Progress in Ultrafast Intense Laser Science II Springer Series in Chemical Physics Volume 85*; Yamanouchi, K., Chin, S. L., Agostini, P., Ferrante, G., Eds.; Springer, 2007; pp 25–41.
(30) Liu, M.; Wu, C.; Wu, Z.; Yang, H.; Gong, Q.; Huang, W.; Zhu, T. *J. Am. Soc. Mass Spectrom.* **2010**, *21*, 1122–1128.
(31) Hankin, S. M.; Villeneuve, D. M.; Corkum, P. B.; Rayner, D. M. *Phys. Rev. Lett.* **2000**, *84* (22), 5082–5085.
(32) Itakura, R.; Watanabe, J.; Hishikawa, A.; Yamanouchi, K. *J. Chem. Phys.* **2001**, *114*, 5598–5606.
(33) Schreiner, J.; Voigt, C.; Mauersberger, K.; McMurry, P.; Ziemann, P. *Aerosol Sci. Technol.* **1998**, *29* (1), 50–56.
(34) Schreiner, J.; Schild, U.; Voigt, C.; Mauersberger, K. *Aerosol Sci. Technol.* **1999**, *31* (5), 373–382.
(35) Wang, X.; Kruis, F. E.; McMurry, P. H. *Aerosol Sci. Technol.* **2005**, *39* (7), 611–623.
(36) Cziczo, D. J.; Thomson, D. S.; Murphy, D. M. *Science* **2001**, *291* (5509), 1772–1775.
(37) Spencer, M. T.; Prather, K. A. *Aerosol Sci. Technol.* **2006**, *40* (8), 585–594.
(38) Reents, W. D.; Ge, Z. *Aerosol Sci. Technol.* **2000**, *33* (1-2), 122–134.
(39) Murphy, D. M.; Hudson, P. K.; Cziczo, D. J.; Gallavardin, S.; Froyd, K. D.; Johnston, M. V; Middlebrook, A. M.; Reinard, M. S.; Thomson, D. S.; Thornberry, T.; Wexler, A. S. *Atmos. Chem. Phys.* **2007**, *7* (12), 3195–3210.
(40) Zhou, L.; Park, K.; Milchberg, H. M.; Zachariah, M. R. *Aerosol Sci. Technol.* **2007**, *41* (9), 818–827.
(41) Zawadowicz, M. A.; Proud, S. R.; Seppalainen, S. S.; Cziczo, D. J. *Atmos. Chem. Phys.* **2015**, *15* (15), 8975–8986.

Insert Table of Contents artwork here